

Characterization of the Photosynthetic Apparatus and Proteome of *Roseobacter denitrificans*

Kai Tang · Rui Zong · Fan Zhang ·
Na Xiao · Nianzhi Jiao

Received: 30 June 2009 / Accepted: 16 September 2009 / Published online: 14 October 2009
© Springer Science+Business Media, LLC 2009

Abstract The phototrophic capacity of aerobic anoxygenic phototrophic bacteria endows them with a selective advantage over other heterotrophic bacteria in the oligotrophic ocean. Here, we reported the phototrophic features and proteome of an aerobic phototrophic bacterium *Roseobacter denitrificans* under starvation stress. The fluorescence induction and relaxation measurements suggested that the photosynthetic capacity in *R. denitrificans* was preserved but was lower than in the photoautotrophic bacterium *Rhodobacter sphaeroides*. The existence of light-harvesting complexes (LH1 and LH2) and the reaction center (RC) in the native membrane were demonstrated through atomic force microscopy image analysis as direct evidence of their phototrophy. The homology-based LH1–RC complex structure was proposed in which RC was the *Rb. sphaeroides* homolog structure surrounded by the LH1. Moreover, the protein expression profiles of cells in the stationary phase under heterotrophic and mixotrophic conditions show that light enhanced or activated some proteins such as carbon monoxide dehydrogenase and NifU to cope with the low levels of amino acids and carbon sources under starvation conditions.

Introduction

Aerobic anoxygenic phototrophic bacteria (AAPB) are a group of heterotrophic bacteria with the capability of phototrophy and which appear to have a particular role in the ocean's carbon cycling [3, 13]. Because, bacterial

chlorophyll *a* (BChl*a*)-based phototrophic function make AAPB more competent in oligotrophic environments where dissolved organic matter is sparse, the relative abundance of AAPB compared to total bacteria is expected to be higher in oligotrophic waters [8, 10, 11]. AAPB in such environments are frequently exposed to the limitations of various nutrients and reduced light conditions, which lead to AAPB showing a somewhat stationary survival rather than exponential growth [18]. Light and carbon availability in nutrient-depleted environments greatly influence the evolutionary selection of AAPB because of their phototrophic and heterotrophic abilities [10, 18].

Most of AAPB strains belong to the *Roseobacter* clade, which is the second largest marine picoplankton lineage [1]. *Roseobacter denitrificans* is used as a representative aerobic phototrophic bacterium to investigate diverse processes such as phototrophy, since it allows physiological, biochemical as well as genetic assays [16, 19, 28, 32]. In AAPB, anoxygenic phototrophy is a central metabolic process. The *R. denitrificans* photosynthetic genes are similar to those of the well-studied photoautotrophic bacteria such as *Rhodobacter (Rb.) sphaeroides*. Therefore, *R. denitrificans* is particularly suitable as a model in deciphering the structure–function relationships and strategies of the AAPB phototrophy machinery. In comparison to oxygenic phototrophs, the anoxygenic bacteria photosynthetic apparatus consists of a reaction center (RC) complex and two light-harvesting complexes (LH1 and LH2). The LH1 complex is generally thought to consist of about 16 heterodimeric protein subunits (α and β), which possibly form a ring around the RC, and the LH2 complexes display a similar architecture with the eight or nine α , β -heterodimers cyclically arranged. The structural proteins for LH1, LH2, and the RC are encoded by the *puf*, *puc*, and *puh* genes, respectively. The LH1 and LH2 using carotenoids

K. Tang · R. Zong · F. Zhang · N. Xiao · N. Jiao (✉)
National Key Laboratory of Marine Environmental Sciences,
Xiamen University, Xiamen 361005, China
e-mail: jjiao@xmu.edu.cn; jiaolab@gmail.com

and BChl a as photoreceptors absorb and channel light energy and transfer it to the RC. Due to their central role in phototrophy, the detailed structural information about LH complexes in various species of purple bacteria is emerging [15, 22, 25]. The crystal structure of the complete LH1–RC complex from *Rhodospseudomonas (Rps.) palustris* has been revealed by X-ray crystallography [22]. Apart from crystal structure determinations, the basic structure of the photosystem and its individual components has also been elucidated by cryoelectron microscopy and atomic force microscopy (AFM) approaches [15, 25]. The AFM technique is effectively employed in some studies for visualizing the bacterial photosystem close to physiological conditions, i.e., in buffer solution, at room temperature, and under normal pressure [2, 23]. Despite the applications of AFM to some purple bacteria photosystems in recent years, to our knowledge, few AFM studies have been reported on the photosynthetic apparatus of AAPB.

The genome data indicate that *R. denitrificans* is a mixotrophic organism which acquires the energy necessary for growth and reproduction through a combination of phototrophy and heterotrophy [32]. This article reports the phototrophic features and apparatus of *R. denitrificans* in the stationary phase under starvation stress conditions using fluorescence induction and relaxation (FIRE) [12], AFM, and bioinformatics approaches. Furthermore, to investigate the effect of phototrophy on the growth of *R. denitrificans*, a comparative proteomic approach was used to detect the changes in protein expression of stationary phase cells after illumination. This study will contribute to a better understanding of the adaptations of *R. denitrificans* to nutrient starvation.

Materials and Methods

Strains and Culture Conditions

Roseobacter denitrificans (DSM 7001) was maintained and precultured aerobically at 25°C with RO medium as previously [29], and stirred at a rate of 160 rpm in the dark. Growth was monitored by measuring the optical density (OD) at 600 nm (OD₆₀₀) with FLEXstation (Molecular Device, USA). To establish the starvation-induced stationary phase, the feed of medium to the chemostat was switched off during the steady state. Cells at the end of exponential growth (OD₆₀₀ of ≈ 2.9) were diluted into 30 vol of sterile seawater. The diluted suspensions were incubated for 30 h in dark, and then the effect of light on the cell suspension was determined under continuous cool white light (low light intensity 30 $\mu\text{E m}^{-2} \text{s}^{-1}$) in a growth chamber (Convicon, Canada) with shaking at 120 rpm for 24 h. For the dark control, the bottle was wrapped tightly

by aluminum foil, which was further for proteomics analysis. The stationary phase samples were taken after the cell density had reached a constant value. Cells were collected and centrifuged at 10000 $\times g$ for 20 min at 4°C using an Eppendorf 5810R centrifuge (Hamburg, Germany). *Rb. sphaeroides* (DSM 158) and *Roseobacter* JL34 (isolated from the East China Sea in our laboratory) were used in this study. *R. JL34* was cultured in the same conditions as above to obtain stationary phase cells, and *Rb. sphaeroides* cultures were grown semi-aerobically in Sistrom's minimal medium [31] at a light intensity of 30 $\mu\text{E m}^{-2} \text{s}^{-1}$.

FIRE Measurements

The FIRE fluorometer system (Satlantic, USA) was used to measure in vivo a range of photo-physiological parameters at high sensitivity. The FIRE protocol involved a strong flash of saturating green (550 nm central wavelength, 30 nm bandwidth), initiating a rise in fluorescence in vivo from an initial value (F_0) to a maximum value (F_M) in a single photosynthetic turnover in 200 μs . The fluorescence signals were separated by the infrared filter (880 nm, 50 nm bandwidth) for BChl a fluorescence. The average signals were obtained from 30 iterations of one sample. Sea water pressed through a 0.2-mm filter was used as a blank for the sample signal. The photochemical quantum yield of primary charge separation (F_V/F_M), functional absorption cross section (σ), and electron transfer turnover of the RC were calculated from the FIRE profiles based on the aquatic photosynthesis biophysical model [14].

Isolation of Photosynthetic Membrane

Cells growing in the light were harvested and washed with 10 mM Tris–HCl, pH 7.5 before being broken through a French pressure cell (30 MPa) (Thermo, USA). Lysates were loaded directly onto 5–60% sucrose gradients and centrifuged for 12 h at 200000 $\times g$ in a Hettich ROTINA-38R centrifuge. The fraction containing large membrane fragments was harvested from about a 40% sucrose layer. Sucrose was removed from the samples through dialysis against a sucrose-free buffer. Membrane solutions were kept at 4°C for AFM analysis.

AFM Imaging of Photosynthetic Membrane

Imaging was performed with a commercial Multi Mode Nanoscope3a AFM (Digital Instruments–Veeco, Santa Barbara, USA) equipped with a vertical engagement 100- μm scanner (J-scanner) and oxide-sharpened Si₃N₄ cantilevers (length 100 μm ; $k = 0.09 \text{ N m}^{-1}$; Olympus, Japan). The freshly cleaved mica was covered by 40 μl of adsorption buffer containing 10 mM Tris–HCl, 150 mM

KCl, 20 mM MgCl₂, pH 7.5. Subsequently, the 3 μ l of membrane solution was diluted in tenfold recording buffer (10 mM Tris-HCl, 100 mM KCl, pH 7.5) and absorbed for 30–40 min on freshly cleaved mica. After adsorption, the sample was gently washed with recording buffer to remove membranes that were not attached firmly to the substrate. The AFM was operated in a contact mode at minimal loading forces (<100 pN). Trace and retrace signals were recorded simultaneously at line frequencies ranging between 4.0 and 7.0 Hz. A detailed description of the data acquisition is described in references [23, 24].

Sequence Analysis and Homology Modeling

Comparative analysis of AAPB photosynthetic apparatus protein sequences was taken from the marine Roseobacter bacteria genome database Roseobase (<http://www.roseobase.org/>). The basic steps in the construction of an LH1-RC model based on comparative homology modeling are amino acid sequence alignment, copying LH1-RC coordinates, and finally refinement. Models were constructed by comparative modeling using the molecular simulation program Modeler v8.0 [6] and were carried out on a Dell Precision 490 workstation. The amino acid sequence alignments were done using Blastp or ClustalW as previously described [6].

Firstly, structures of the LH1 α and β polypeptides in *R. denitrificans* were determined by means of homology modeling using *Rhodospirillum rubrum* LH1 β (PDB entry **1wrg**) [35] and *Rb. sphaeroides* β (PDB entry **1dx7**) [5] as a template, respectively. The transmembrane and extramembrane regions were identified using sequence homology and secondary structure identity as search criteria. Since the sequence similarity between the protein subunits of *Rb. sphaeroides* and *R. denitrificans* RC is very high (see Table 2), the high-resolution structures of RC from *Rb. sphaeroides* [4] (PDB entry **2rcr**) was chosen as a template for comparative homology modeling to predict the structures of RC in *R. denitrificans*.

The only complete crystal structure of LH1-RC of *Rps. palustris* is available to date in photosynthetic purple bacteria [22], so the *R. denitrificans* LH1-RC complex was modeled based on the initial coordinates for LH1-RC complex copied from *Rps. palustris* (PDB entry **1pyh**) [22] by mapping the homologous *R. denitrificans* amino acid sequence onto the *Rps. palustris* structure. The α - and β -polypeptides were aggregated into a circular hexadecameric complex by means of mapping into LH1 of *Rps. palustris* consisting of 16-fold symmetry axis. The two conserved histidines near the carboxy termini of the α - and β -polypeptides in LH1 were widely considered as ligands of the two BChl_a for photosynthetic purple bacteria [5]. Therefore, the proper ligation between the Mg atoms of the

Bchl_a and the highly conserved histidine residues in the α - and β -polypeptides in LH1 was ensured during the mapping.

Finally, the RC structure was placed inside the LH1 ring in the same orientation and locations as observed in *Rps. palustris* [22] and was allowed to rotate and translate as a rigid body. Energy minimization was subsequently performed on LH1-RC under the constraint of a 16-fold symmetry axis. The conformation and relative locations of the pigments were not changed during modeling. The final models were evaluated using PROCHECK [17] and Prosa 2003 [34]. The best model was retained for the analysis. All figures were prepared using the program VMD [9]. A PDB format of the LH-RC used in this study is available upon request.

Proteome Analysis Using Two-Dimensional Gel Electrophoresis

To prepare protein samples for two-dimensional gel electrophoresis (2D GE), the cell pellets were resuspended in 1 ml of lysis buffer (7 M urea, 2 M thiourea, 2% CHAPS, 1% DTT, 4% TRITON-X 100, 2% carrier ampholytes, 5% protease inhibitor cocktail), and then sonicated on ice. The fraction of soluble proteins was yielded by centrifugation. Proteins in the supernatant were precipitated using trichloroacetic acid (TCA)/acetone, and then resuspended in lysis buffer. The concentration of protein was determined using the 2D Quant Kit (GE Healthcare, USA). The 2D GE analysis was performed as previously described [7]. In brief, for the first dimension, isoelectric focusing (IEF), approximately 80 μ g of proteins was loaded onto each precast 18 cm immobilized non-linear pH 3–11 or 4–7 strip (Bio-Rad Laboratories, CA, USA). The strips were rehydrated for 12 h, and IEF was carried out in an Ettan IPG-phor3 System (GE Healthcare). The second dimension, SDS-PAGE, was carried out on 12% polyacrylamide gels in an Ettan DALT apparatus (GE Healthcare). To analyze the reproducibility of 2D gels, we repeated the experiments thrice for each sample. Proteins were visualized using silver staining and scanned with an Image Scanner II system (Amersham, USA). Images were analyzed and quantitatively compared using PDQuest 8.0 Software (Bio-Rad Laboratories). Of the proteins detected in *R. denitrificans* proteome by PDQuest software, 12 protein spots that increased significantly in abundance in the samples cultured in light gels were identified by mass spectrometry (MS).

Protein Identification Using MS

Protein spots of interest were cut from the silver-stained gels and were detained with a solution of 15 mM

potassium ferricyanide and 50 mM sodium thiosulfate (1:1) for 20 min at room temperature. Then the samples were washed twice with deionized water, shrunk by dehydration in acetonitrile (ACN). The samples were then swollen in a digestion buffer containing 20 mM ammonium bicarbonate and 12.5 ng l⁻¹ trypsin at 4°C (Promega, USA) and peptides were extracted twice using 5% trifluoroacetic acid (TFA) in 50% ACN. The extracts were dried under the protection of N₂. MALDI-TOF/TOF-MS analysis was carried out in Explorer 4700 Proteomics Analyzer (Applied Biosystems, USA). Peptides were eluted onto the target with 0.7 µl matrix solution (α -cyano-4-hydroxycinnamic acid in 0.1% TFA, 50% ACN). Samples were allowed to air to dry before inserting them into the mass spectrometer. All data MS/MS searches were performed using MASCOT version 2.1 (Matrix Science, UK). The settings were used: NCBI nr database (release 20070627; 4182491 sequences; 1439956234 residues), bacteria, trypsin digest with one missing cleavage, peptide tolerance of ± 0.2 Da, fragment mass tolerance of ± 0.3 Da, and possible oxidation of methionine.

Results and Discussion

Phototrophic Features and Architecture of the Photosynthetic Apparatus

As a first step toward illustrating *R. denitrificans* phototrophy characteristics, FIRE measurements were carried out to determine the photosynthetic parameters that were important for the quantification of phototrophy capacity in AAPB (Fig. 1). These parameters included photochemical

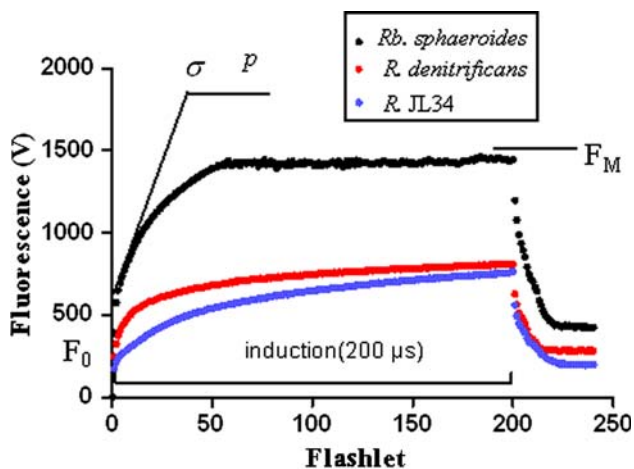


Fig. 1 FIRE fluorescence kinetic transient of *Rb. sphaeroides*, *R. denitrificans*, and *R. JL34* (from top to bottom) elicited upon 530 nm excitation. F_0 and F_M minimal and maximal fluorescence yields, p connectivity, σ functional absorption cross section

efficiency (F_V/F_M) which was an indicator for the efficiency of the conversion of light into chemical energy, and the relative functional cross section (σ) which was a comparable estimation of the size of the photosynthetic unit (RC plus LH system) [12]. The green light excitation energy lay in the major absorption area of carotenoid, and thus the $\sigma_{530\text{nm}}$ value reflected the absorption in both LH1- and LH2-bound carotenoids.

All three strains (*R. denitrificans*, reference bacteria *R. JL34* and *Rb. sphaeroides*) responded to green excitation (530 nm) with variable Bchl_a fluorescence in 880 nm (Fig. 1). They were characterized as purple non-sulfur phototrophic bacteria with a similar LH1–RC and LH2. The strains displayed a similar efficiency of carotenoid and Bchl_a to photosynthetic apparatus energy transfer (F_V/F_M) at around 0.7–0.8, suggesting that they all had high efficiency of primary photochemistry in the bacterial photosynthetic apparatus. However, they differed in the rate of the rapid fluorescence induction process, an indication of the different sizes ($\sigma_{530\text{nm}}$) of the photosynthetic units (relative functional cross section) (Table 1). Particularly, the fluorescence induction kinetic curve for *R. JL34* did not completely reach the saturation plateau by the end of the single turnover flash (STF) even when the duration of STF was set to 200 µs (Fig. 1). The result suggested that *R. JL34* did not saturate the variable fluorescence under the excitation power available in the FIRE system, possibly due to the small size of the photosynthetic unit ($\sigma_{530\text{nm}}$). However, the photosynthetic unit in *R. denitrificans* only showed a slightly smaller size (σ) than in *Rb. sphaeroides*. The connectivity factor of the transfer ring of excitation energy efficiency (p) between photosynthetic units was estimated to be approximately 0.07 in *R. denitrificans*, much lower than in *Rb. sphaeroides*. Collectively, these results indicated that *R. denitrificans* had the lower photosynthetic capacity when compared to photoautotrophic bacteria. In fact, *R. denitrificans* and *R. JL34* were AAPB isolated from the surface ocean where the irradiation was normally saturated, whereas *Rb. sphaeroides* was a photoautotrophic bacterium which preferred to live in the bottom of aquatic environments where the light availability was significantly reduced [1]. To survive with low light, *Rb. sphaeroides* developed a significantly higher photosynthetic capacity.

Table 1 Comparative photosynthetic parameters determined by FIRE

Organism	F_V/F_M	$\sigma_{530\text{nm}}$ (Å ²)	P
<i>Rb. sphaeroides</i>	0.78 ± 0.02	108 ± 2	0.25 ± 0.04
<i>R. denitrificans</i>	0.75 ± 0.01	95 ± 5	0.07 ± 0.01
<i>R. JL34</i>	0.77 ± 0.02	73 ± 3	0.06 ± 0.01

All the strains were grown under light-adapted starvation stress conditions. The experiment was performed three times, and the means ± standard errors of the mean are shown

To visualize the supramolecular architecture of the photosynthetic membrane related directly to phototrophy, native membrane was adsorbed to freshly cleaved mica and imaged by AFM in buffer solution. The AFM results provided direct evidence for photosynthetic protein expression in *R. denitrificans* under starvation stress conditions. The AFM topography of the sample recorded in buffer solution clearly showed the structure of the polypeptide loops in native membranes as shown in Fig. 2. This was invaluable since AFM provided a way to measure the heights of the complexes above the membrane (Fig. 2a, b). On the cytoplasmic side, the height from the lipid bilayer to the highest point of the protruding RC was approximately 45 Å ($n = 20$), and from the highest point on the LH1 ring to the highest point of the RC was approximately 21 Å ($n = 20$). On the periplasmic side, the distance from the surface of the LH1 complex to the membrane bilayer was approximately 24 Å ($n = 20$). Therefore, given that the measured thickness of the membrane bilayer was approximately 53 Å, the overall height of the LH1–RC complex was approximately 98 Å. These heights together with the section analysis indicated that the protrude domain consisted of a single layer of LH2 and LH1–RC complexes. The variable content of LH2 in the membrane allowed the bacteria to regulate the size of their photosynthetic unit and optimized their light harvesting capacity to adapt to the prevailing light intensity [26, 27]. During low illumination, the amount of LH2 could generally increase to three times the amount of LH1 [26]. The ratio of LH2 to LH1 in the area scanned (Fig. 2c) was about 10 and thus higher than the average value of 7 in the low light-adapted membrane from *Rhodospirillum photometricum* [26]. At higher magnification, the topography of the LH1–RC complex revealed that the RC was surrounded by an elliptical LH1 ring (Fig. 2d, e). Figure 2d, e showed rings with a diameter of ~ 118 Å, which were in close contact with several LH2 rings exhibiting diameters of ~ 50 Å. The diameter of LH1–RC complexes and LH2 in *Rb. sphaeroides* was ~ 125 and ~ 56 Å, respectively, in previous studies [20, 30]. The similar size of photosynthetic unit in two bacteria was also validated from relatively AAPB with the relatively smaller functional absorption cross section of RC ($\sigma_{530\text{nm}}$) by the infrared fluorescence kinetic curve (Table 1).

Photosynthetic genes identified among the eight AAPB genomes available in the *Roseobacter* clade suggested that all components of the LH1–RC and LH2 were structurally conserved with high sequence identities with their homologues of *Rb. sphaeroides* varying from 53 to 90% (Table 2). Several AAPB strains (*Roseobacter* CCS2, *Roseovarius* 217, and *Loktanella vestfoldensis* SKA53) lacked *puc* genes that encode LH2 (Table 2), but *puf* and *puh* genes encoding LH1–RC protein that is required for phototrophy were present in all AAPB. The LH1 α - and

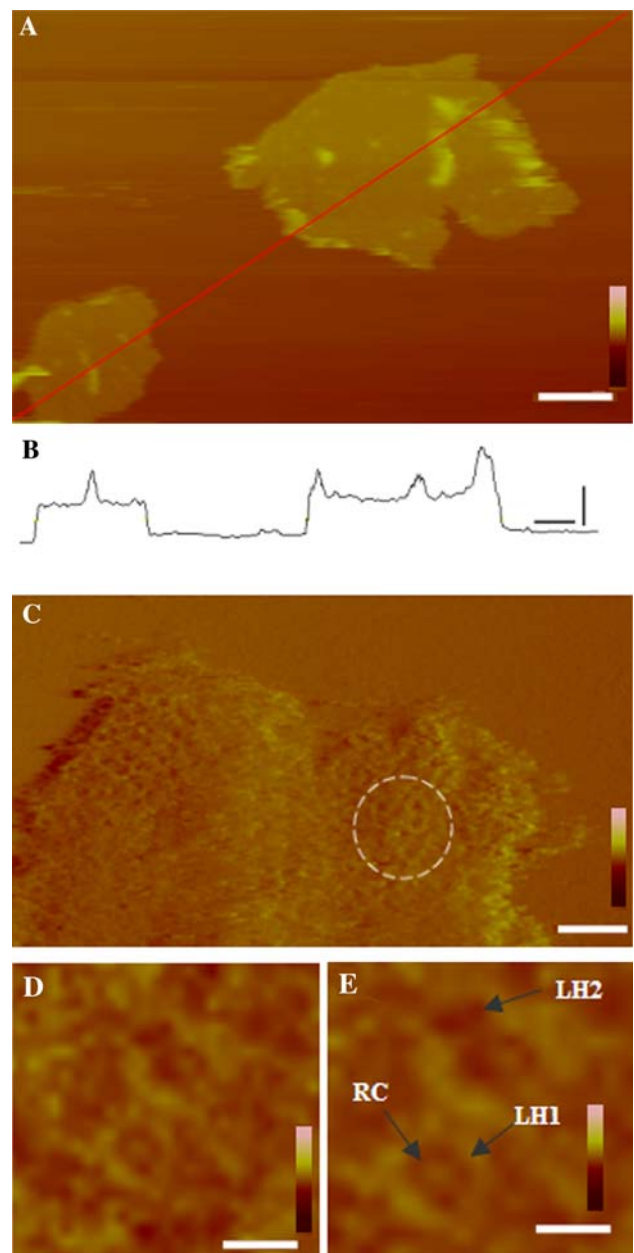


Fig. 2 AFM images of the photosynthetic apparatus. **a** Overview AFM topography of a native membrane of *R. denitrificans* adsorbed to mica. (Scale bar, 300 nm; vertical false-color scale bar, 100 nm.) **b** The height profile along the line in (a) (horizontal scale bar, 100 nm; vertical scale bar, 50 nm). **c** Medium-resolution topography of a native photosynthetic membrane. The circle outlines the assembly of the ring-shaped photosynthetic units. (Scale bar, 80 nm; vertical false-color scale bar, 10 nm.) **d** High-magnification topography of the circle region in (c) (Scale bar, 20 nm; vertical false-color scale bar, 5 nm.) **e** Magnified area of (d) displaying a typical LH1–RC, LH2 (denoted by arrow). (Scale bar, 15 nm; vertical false-color scale bar, 5 nm.)

β -subunits in *R. denitrificans* showed 71 and 84% sequence identities. The putative α - and β -subunits were composed of 54 and 48 amino acid residues, and showed these

Table 2 Percentages of LH and RC amino acid sequences identities between *Rb. sphaeroides* and AAPB in the *Roseobacter* clade

Protein complexes	Gene designation	Gene product	<i>R. denitrificans</i> (%)	<i>Roseobacter litoralis</i> (%)	<i>Roseobacter shibae</i> DFL 12 (%)	<i>Jannaschia</i> sp. CCS1 (%)	<i>Roseobacter</i> sp. CCS2 (%)	<i>Loktanella vesifoldensis</i> SKA53 (%)	<i>Roseovarius</i> sp. 217 (%)	<i>Hoeflea phototrophica</i> DFL-43 (%)
LH1-RC	<i>pufA</i>	Light-harvesting protein B-875, alpha chain	71	71	75	64	65	66	77	52
	<i>pufB</i>	Light-harvesting protein B-875, beta chain	84	84	90	82	71	74	82	45
	<i>pufL</i>	Photosynthetic reaction center L subunit	71	71	73	66	70	73	74	67
	<i>pufM</i>	Photosynthetic reaction center M subunit	62	61	66	65	73	72	69	63
	<i>pufA</i>	Photosynthetic reaction center H subunit	56	56	58	53	59	56	55	40
LH2	<i>pucA</i>	Light-harvesting protein B-800/850, alpha chain	50	52	50	63	-	-	-	59
	<i>pucB</i>	Light-harvesting protein B-800/850, beta chain	70	70	74	72	-	-	-	31

-, signifies LH2 complex is absent

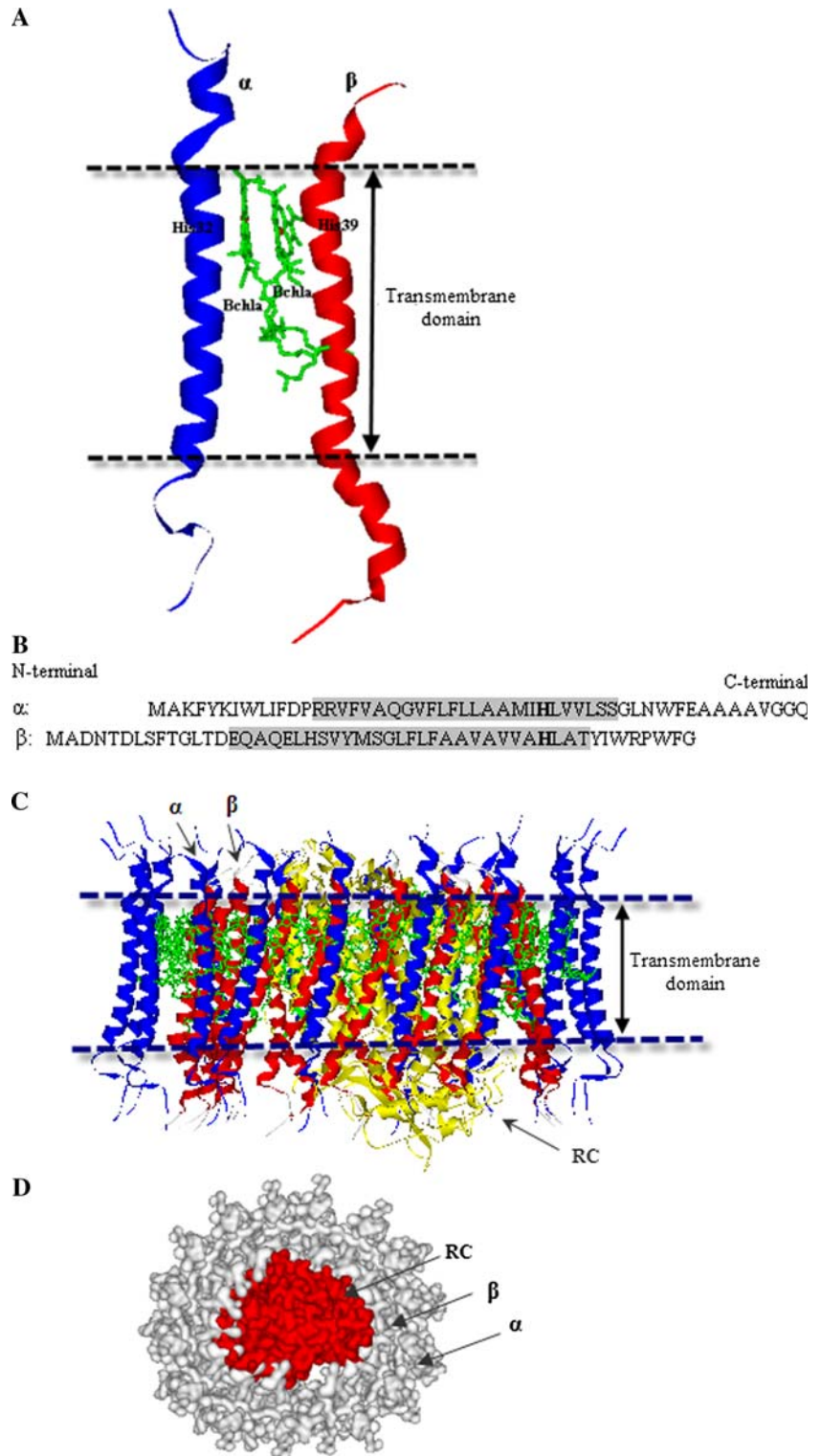
residues were well conserved, including the histidine residues presumed to bind 2 Bchl_a (32nd and 39th of the α and β subunits, respectively) (Fig. 3a). Both α - and β -polypeptides consisted of polar N- and C-termini and a central hydrophobic region as shown in Fig. 3b. The N-termini lay on the cytoplasmic side of the membrane, whereas the C-termini on the periplasmic side. Amino acids in the central hydrophobic region formed two transmembrane α -helices. The model of the complete LH1-RC of *R. denitrificans* showed the RC (the *Rb. sphaeroides* homolog structure), surrounded by 16 LH1 subunits, which was based on *Rps. palustris* LH1-RC elliptical symmetry (Fig. 3c, d). The overall structures and sequences of the *R. denitrificans* LH1-RC were highly homologous to those previously reported for the LH1-RC of *Rb. sphaeroides*. Furthermore, *R. denitrificans* is the only known AAPB strain that is able to survive under anaerobic denitrifying conditions. *R. denitrificans* may thus represent an intermediate evolutionary form between anoxygenic photoautotrophic bacteria and AAPB.

It was previously suggested that the discontinuous organization of membranes probably resulted in the lower amount of photosynthetic apparatus in AAPB than that in typical anaerobic phototrophic bacteria [36]. Thus, taken together with the findings in this article, these results imply that the apparatus structure and photochemical efficiency (F_V/F_M) of *R. denitrificans* are similar to *Rb. sphaeroides*; however, it exhibited the limited phototrophic activity due to the smaller amount of photosystem proteins and the lower transfer energy efficiency (p) between these apparatuses. Under starvation stress, expression of photosynthetic apparatus may present an ecological advantage over strictly heterotrophic bacteria, possibly increasing the competitiveness, and the survival rates of *R. denitrificans*.

Comparative Proteomics Analysis for Bacteria Grown Under Heterotrophic and Mixotrophic Conditions

Roseobacter denitrificans is capable of photosynthetic light utilization under carbon starvation as shown above. We found that the presence of the light (mixotrophic growth) induced a relatively higher growth rate than in the dark (heterotrophic growth) for *R. denitrificans*, determined from the OD (data not shown). To examine the influence of anoxygenic phototrophy on the growth of the *R. denitrificans*, the response in protein expression and identified proteins of interest were studied when *R. denitrificans* was subjected to the limited nutrition sources in the light and dark, respectively. A proteomic view of *R. denitrificans* during the stationary phase of culture in the presence and absence of light is presented in Fig. 4a, b, and it can be observed that more than 80% of the soluble proteins fall into the pH range 4–6. The proteome analyzed on 2D gels

Fig. 3 Model of the LH1–RC complex in *R. denitrificans*. **a** An illustration of an elementary subunit of the LH1 complex in side view. The α -polypeptides (left), β -polypeptides (right), and photosynthetic pigments (middle) are shown. The central Mg-atoms of BChl a are displayed with a ball model ligated to the histidine. **b** The amino acid sequences of α - and β -polypeptides of LH1. The hydrophobic region is marked in gray. The numbering specifies the amino acid position relative to the His (bold), which binds the central Mg $^{2+}$. **c** Side view of the LH1–RC complex. The RC shown with an arrow is the *Rb. sphaeroides* homolog structure surrounded by the LH1 complex. The α - and β -subunit of LH1 with an arrow is shown, respectively. The relative heights of the RC and LH1 complexes and their positions in the membrane were obtained from the AFM data in this article. **d** Top view of the LH1–RC complex shown as a soft surface model. The RC subunits (middle), the α - and β -apoproteins of LH1 are denoted by arrows



showed proteins differentially expressed by *R. denitrificans*, from which protein spots were further identified by combining MS and bioinformatics tools. We selected 12 proteins for sequencing based on their resolution and consistency in repeated gels (denoted by arrows, Fig. 4).

The proteins that were selected for sequencing were almost not detected in the control sample from cells in the dark.

Table 3 presents the proteins identified in this study, indicating some novel metabolic pathways for *R. denitrificans* from the sequenced genome directly. Strikingly, the

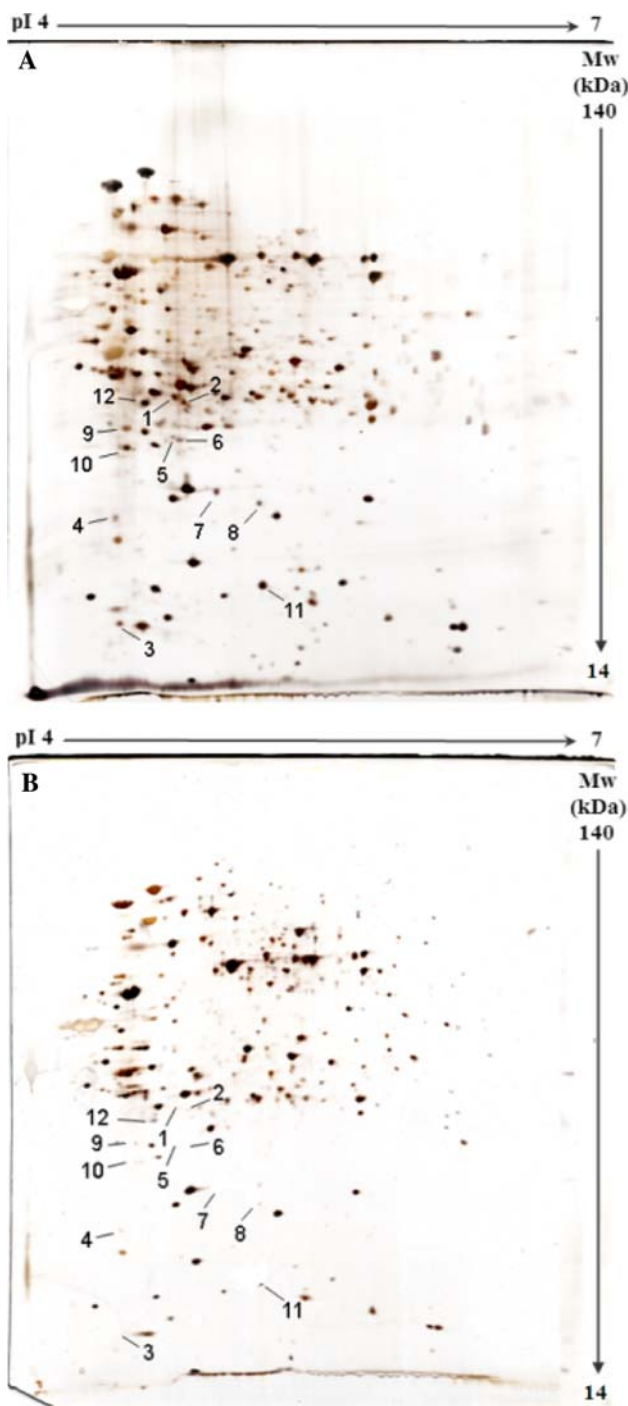


Fig. 4 Silver-stained 2D gel images (pH 4–7) of soluble proteins from *R. denitrificans* at the stationary phase when grown in the presence (a) and absence of light (b). Only the well-resolved differential protein spots (1–12) that altered in light conditions were labeled and excised from the gel for protein characterization as reported in Table 3

genome of *R. denitrificans* reveals the presence of the carbon monoxide dehydrogenase complex, which has the ability to use CO as both the carbon and energy sources [32]. However, the genome lacks the *RuBisCO* gene that

encodes the key Calvin cycle enzyme ribulose diphosphate carboxylase for known photoautotrophic carbon fixation pathways (CO₂ fixation) [32]. Here, the carbon monoxide dehydrogenase (spot no. 11, Table 3) was identified that can oxidize CO. By carbonic anhydrase, the production of CO₂ was attached to phosphoenolpyruvate, or pyruvate to form oxaloacetate. The fixed carbon was recruited into the TCA cycle, or other pathways which could produce amino acid or pyrimidine nucleotide. In many *Roseobacter* clade bacteria, carbon monoxide dehydrogenase is involved in the cycling of CO in the marine environment [33]. The increased level of glycerol-3-phosphate-binding periplasmic protein precursor (spot no. 5, Table 3) indicated that the active transport of glycerol-3-phosphate was induced by light. The complex was composed of two ATP-binding proteins, and by ATP hydrolysis the two subunits provided the energy for the accumulation of substrate against the concentration gradient. In line with this, ubiquinol-cytochrome *c* reductase (spot no. 9, Table 3) also increased to generate a proton gradient by electron transport, and this implied an enormous source of potential energy for ATP synthesis. The upregulated enzyme of 3-oxoadipate CoA-succinyl transferase (spot no. 10, Table 3) produced succinate to provide enough intermediate energy for the TCA cycle [32]. These proteomic changes in conjunction with the markedly enhanced respiratory capacity and the active small molecular substrate transport suggested a significant upregulation of organic carbon uptake during growth under illumination. Therefore, light not only can supply extra energy for AAPB, but can also enhance carbon utilization ability.

The other major proteins expressed differentially in the dark and light growth conditions included: NifU (spot no. 7, Table 3) related to the nitrogen-fixation process, thioredoxin (spot no. 3, Table 3) and immunogenic protein (spot no. 12, Table 3). The NifU was thought to be involved in synthesizing the iron–sulfur metalloclusters required for nitrogen fixation [37]. The thioredoxin and immunogenic protein also showed higher expression in the light than in the dark. Previous studies have demonstrated that thioredoxin is essential for cell growth and possibly is also involved in regulating anoxygenic photosynthetic gene expression [21]. Immunogenic protein was expected to be functional in protecting the cell from outer damage and possibly to repair damaged proteins during the stationary phase.

Interestingly, it was found that there is no significant difference between the proteomic profiles of *R. denitrificans* from growth with the nutrient-enriched culture medium under dark and light conditions (data not shown). Furthermore, the growth rate of *R. denitrificans* was slightly influenced by the low light intensity. *R. denitrificans* might depend on carbon sources rather than light in its exponential growth phase. The maps of *R. denitrificans* proteomics were more complicated than the ones in limited

Table 3 Proteins identified by MS/MS (MALDI-TOF/TOF)

Spot no. ^a	Gene ID ^b	Protein name	Theo. pI/mass (kDa) ^c	Exp. pI/mass (kDa) ^d	Sequence coverage (%) ^e	MASCOT score
1	gil110679475	Hypothetical protein	4.8/35	4.7/31	47	412
2	gil110681034	Tryptophan synthase	4.7/28	4.8/29	30	348
3	gil110677843	Thioredoxin	4.3/12	4.4/16	58	176
4	gil110679605	YceI-like family protein	4.6/18	4.4/20	34	263
5	gil110680140	Glycerol-3-phosphate-binding periplasmic protein precursor	4.4/45	4.6/25	18	150
6	gil110680358	Hypothetical protein	4.3/21	4.7/24	44	500
7	gil110678955	NifU	4.9/21	4.8/20	59	239
8	gil110681334	Hypothetical protein	5.0/17	5.0/19	74	382
9	gil110677947	Ubiquinol-cytochrome c reductase	4.6/20	4.5/24	45	360
10	gil110679403	3-Oxoacid CoA-succinyl transferase	4.4/22	4.5/23	34	414
11	gil110680173	Carbon monoxide dehydrogenase	5.0/17	5.0/17	17	104
12	gil110678837	Immunogenic protein	4.6/33	4.6/30	38	150

^a Spot numbers are identical to those given in Fig. 4

^b Accession number in NCBI nr

^c Theoretical pI and molecular weight

^d Experimental pI and molecular weight

^e Number of peptides identified by MS/MS/sequence percentage coverage

organic medium. It was implied that *R. denitrificans* would turn off part of pathways and remain key enzymes of energy metabolism for bacteria survive under severe nutrient-limited conditions. For successful survival and growth, photosynthetic organism *R. denitrificans* could adjust their phototrophic and heterotrophic dependence to maximize the energy acquisition and metabolic efficiency under carbon starvation.

Acknowledgments Professor John Hodgkiss is thanked for his help with English. This study was supported by the MOST Project 2007CB815904; NSFC 40632013; COMRA DYXM-115-02-4-3; SOA 200805068 and PhD programs foundation of Ministry of Education of China 200803841021.

References

- Allgaier M, Uphoff H, Felske A et al (2003) Aerobic anoxygenic photosynthesis in *Roseobacter* clade bacteria from diverse marine habitats. *Appl Environ Microbiol* 69:5051–5059
- Bahatyrova S, Frese RN, Siebert CA et al (2004) The native architecture of a photosynthetic membrane. *Nature* 430:1058–1062
- Beja O, Suzuki MT, Heidelberg JF et al (2002) Unsuspected diversity among marine aerobic anoxygenic phototrophs. *Nature* 415:630–633
- Chang CH, El-Kabbani O, Tiede D et al (1991) Structure of the membrane-bound protein photosynthetic reaction center from *Rhodobacter sphaeroides*. *Biochemistry* 30:5352–5360
- Conroy MJ, Westerhuis WH, Parkes-Loach PS et al (2000) The solution structure of *Rhodobacter sphaeroides* LH1 beta reveals two helical domains separated by a more flexible region: structural consequences for the LH1 complex. *J Mol Biol* 298:83–94
- Eswar ND, Eramian B, Webb Shen MY et al (2008) Protein structure modeling with MODELLER. *Methods Mol Biol* 426:145–159
- Gade D, Gobom J, Rabus R (2005) Proteomic analysis of carbohydrate catabolism and regulation in the marine bacterium *Rhodospirillum rubrum*. *Proteomics* 5:3672–3683
- Hu YH, Du HL, Jiao NZ et al (2006) Abundant presence of the γ -like Proteobacterial pufM gene in oxic seawater. *FEMS Microbiol Lett* 263:200–206
- Humphrey W, Dalke A, Schulten K (1996) VMD: visual molecular dynamics. *J Mol Graph* 14:33–38
- Jiao NZ, Zhang Y, Zeng YH et al (2007) Distinct distribution pattern of abundance and diversity of aerobic anoxygenic phototrophic bacteria in the global ocean. *Environ Microbiol* 9:3091–3099
- Koblizek M, Masin M, Ras J et al (2007) Rapid growth rates of aerobic anoxygenic phototrophs in the ocean. *Environ Microbiol* 9:2401–2406
- Koblizek M, Shih JD, Breitbart SI et al (2005) Sequential assembly of photosynthetic units in *Rhodobacter sphaeroides* as revealed by fast repetition rate analysis of variable bacteriochlorophyll a fluorescence. *Biochim Biophys Acta* 1706:220–231
- Kolber ZS, Plumley FG, Lang AS et al (2001) Contribution of aerobic photoheterotrophic bacteria to the carbon cycle in the ocean. *Science* 292:2492–2495
- Kolber ZS, Prasil O, Falkowski PG (1998) Measurements of variable chlorophyll fluorescence using fast repetition rate techniques: defining methodology and experimental protocols. *Biochim Biophys Acta* 1367:88–106
- Konorty M, Kahana N, Linaroudis A et al (2008) Structural analysis of photosynthetic membranes by cryo-electron tomography of intact *Rhodospirillum rubrum* cells. *J Struct Biol* 161:393–400
- Kortlüke C, Breese K, Gad'on N et al (1997) Structure of the puf operon of the obligately aerobic, bacteriochlorophyll alpha-containing bacterium *Roseobacter denitrificans* OCh114 and its expression in a *Rhodobacter capsulatus* puf puc deletion mutant. *J Bacteriol* 179:5247–5258
- Laskowski RA, Rullmann JA, MacArthur MW et al (1996) AQUA and PROCHECK-NMR: programs for checking the quality of protein structures solved by NMR. *J Biomol NMR* 8:477–486
- Li Q, Jiao NZ, Peng ZQ (2006) Environmental control of growth and BChl a expression in an aerobic anoxygenic phototrophic bacterium *Erythrobacter longus* (DSMZ6997). *Acta Oceanol Sin* 25:138–144
- Nishimura K, Shimada H, Shinmen T et al (1999) Photosynthetic regulatory gene cluster in an aerobic photosynthetic bacterium *Roseobacter denitrificans*. *J Gen Appl Microbiol* 45:129–134

20. Olsen JD, Tucker JD, Timney JA et al (2008) The organization of LH2 complexes in membranes from *Rhodobacter sphaeroides*. *J Biol Chem* 283:30772–30779
21. Pasternak C, Haberzettl K, Klug G (1999) Thioredoxin is involved in oxygen-regulated formation of the photosynthetic apparatus of *Rhodobacter sphaeroides*. *J Bacteriol* 181:100–106
22. Roszak AW, Howard TD, Southall J et al (2003) Crystal structure of the RC-LH1 core complex from *Rhodospseudomonas palustris*. *Science* 302:1969–1972
23. Scheuring S (2006) AFM studies of the supramolecular assembly of bacterial photosynthetic core-complexes. *Curr Opin Chem Biol* 10:387–393
24. Scheuring S, Goncalves RP, Prima V et al (2006) The photosynthetic apparatus of *Rhodospseudomonas palustris*: structures and organization. *J Mol Biol* 358:83–96
25. Scheuring S, Levy D, Rigaud JL (2005) Watching the components of photosynthetic bacterial membranes and their in situ organisation by atomic force microscopy. *Biochim Biophys Acta* 1712:109–127
26. Scheuring S, Rigaud JL, Sturgis JN (2004) Variable LH2 stoichiometry and core clustering in native membranes of *Rhodospirillum rubrum*. *EMBO J* 23:4127–4133
27. Scheuring S, Sturgis JN (2005) Chromatic adaptation of photosynthetic membranes. *Science* 309:484–487
28. Schwarze C, Carluccio AV, Venturoli G et al (2000) Photo-induced cyclic electron transfer involving cytochrome bc1 complex and reaction center in the obligate aerobic phototroph *Roseobacter denitrificans*. *Eur J Biochem* 267:422–433
29. Shioi Y (1986) Growth-characteristics and substrate-specificity of aerobic photosynthetic bacterium *Erythrobacter* sp. (Och-114). *Plant Cell Physiol* 27:567–572
30. Siebert CA, Qian P, Fotiadis D et al (2004) Molecular architecture of photosynthetic membranes in *Rhodobacter sphaeroides*: the role of PufX. *EMBO J* 23:690–700
31. Sistrom WR (1960) A requirement for sodium in the growth of *Rhodospseudomonas sphaeroides*. *J Gen Microbiol* 22:778–785
32. Swingley WD, Sadekar S, Mastrian SD et al (2007) The complete genome sequence of *Roseobacter denitrificans* reveals a mixotrophic rather than photosynthetic metabolism. *J Bacteriol* 189:683–690
33. Tolli JD, Sievert SM, Taylor CD (2006) Unexpected diversity of bacteria capable of carbon monoxide oxidation in a coastal marine environment and contribution of the *Roseobacter*-associated clade to total CO oxidation. *Appl Environ Microbiol* 72:1966–1973
34. Tomii K, Hirokawa T, Motono C (2005) Protein structure prediction using a variety of profile libraries and 3D verification. *Proteins* 61:114–121
35. Wang ZY, Gokan K, Kobayashi M et al (2005) Solution structures of the core light-harvesting alpha and beta polypeptides from *Rhodospirillum rubrum*: implications for the pigment-protein and protein-protein interactions. *J Mol Biol* 347:465–477
36. Yurkov VV, Beatty JT (1998) Aerobic anoxygenic phototrophic bacteria. *Microbiol Mol Biol Rev* 62:695–724
37. Zhao DH, Curatti L, Rubio LM (2007) Evidence for nifU and nifS participation in the biosynthesis of the iron-molybdenum cofactor of nitrogenase. *J Biol Chem* 282:37016–37025